Volume 17
Number 23
21 June 2025
Pages 13969-14426

Nanoscale

rsc.li/nanoscale

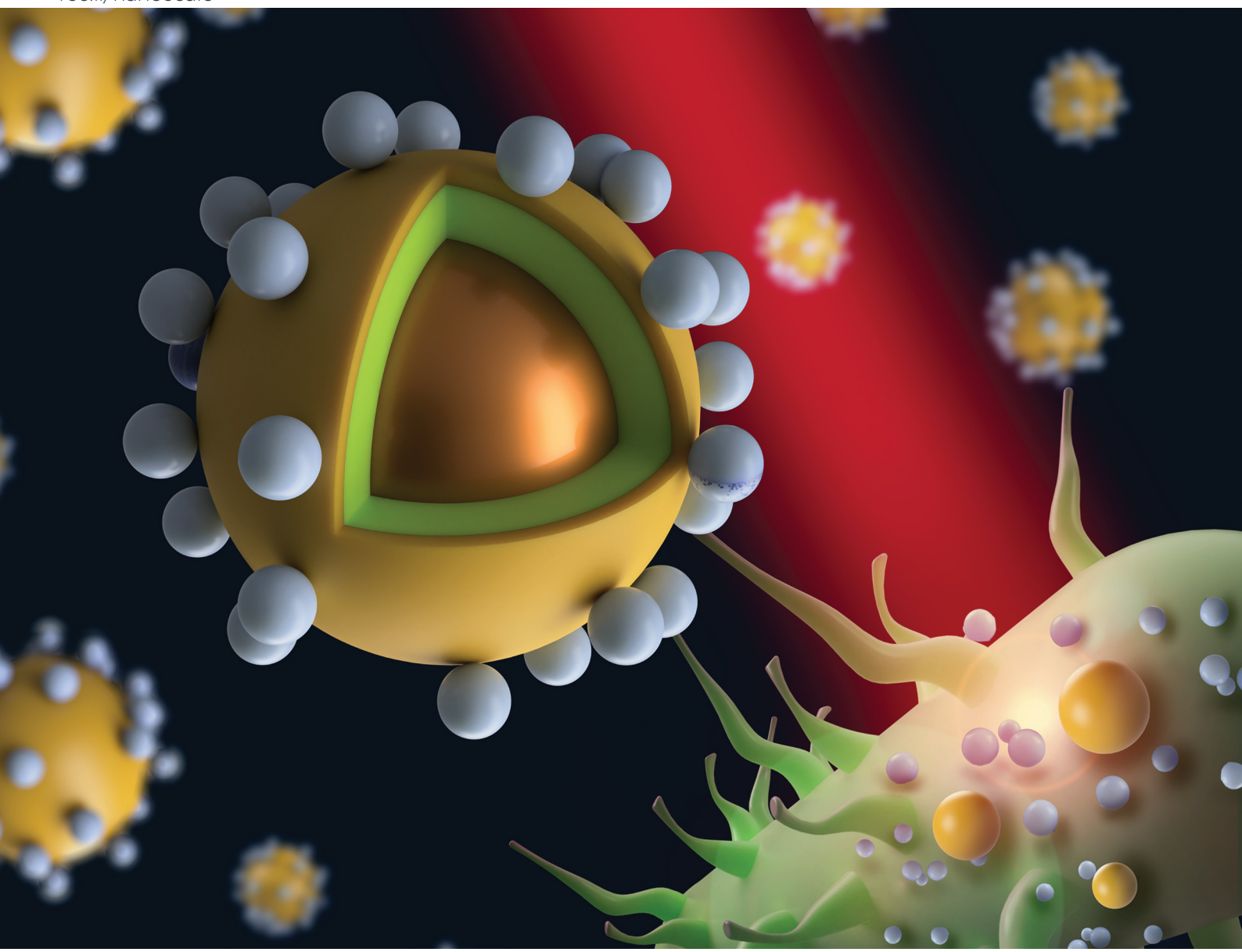

ISSN 2040-3372

ROYAL SOCIETY OF CHEMISTRY

PAPER
Kubra Onbasli, Fusun Can, Alphan Sennaroglu, Mehmet C. Onbasli, Havva Yagci Acar *et al.*
Rational control of combined photothermal and photodynamic therapy for effective eradication of biofilms

NCNST

Nanoscale

PAPER

View Article Online
View Journal | View Issue

Cite this: *Nanoscale*, 2025, **17**, 14145

Rational control of combined photothermal and photodynamic therapy for effective eradication of biofilms†

İrem Koç,‡[a] Kubra Onbasli,‡[b] Cem Kurt,[c] Nazli Atac,[d,e] Francis K. Cooper,[d,e] Kübra Çam,[d,e] Ece Cakir,[a] Rawana Yagan,[c] Fusun Can,[d,e] Alphan Sennaroglu,[a,c,f,g] Mehmet C. Onbasli *[a,c,e,f,g] and Havva Yagci Acar *[a,g,h]

New therapies are essential for eliminating antibiotic-resistant bacteria and their biofilms, which are a major global health threat, causing millions of deaths annually. Here, we demonstrate a combination of photodynamic therapy (PDT) and photothermal therapy (PTT) for the inhibition of biofilms of *Pseudomonas aeruginosa* and *Staphylococcus epidermidis* using aminolevulinic acid (ALA)-loaded polyacrylic acid-coated superparamagnetic iron oxide nanoparticles (PAA-SPIONs) at 200, 600 and 1000 μg mL^{-1} Fe concentrations under 640 nm (0.75 W cm^{-2}), 808 nm (2.6 W cm^{-2}) and 640 + 808 nm (0.75 + 2.6 W cm^{-2}, 20 min) irradiation. PTT experiments indicate ALA/PAA-SPION concentration-dependent heating up to 10.2 °C for PAA-SPIONs and 9.3 °C for ALA/PAA-SPIONs under combined 640 + 808 nm laser excitation. Bacterial growth inhibition by ALA/PAA-SPIONs was investigated with and without laser irradiation for 10 min using 150 and 600 μg Fe per mL or 0.5 mM and 2 mM ALA on both bacterial types. These experiments indicate a 3 to 6-log reduction in *P. aeruginosa* compared to control samples (without nanoparticles or a laser) with increasing Fe and ALA concentrations. Growth was completely inhibited by ALA/PAA-SPIONs under 640 + 808 nm irradiation. ALA/PAA-SPIONs caused growth inhibition of *S. epidermidis* between 2-log and 4-log with increasing wavelengths, Fe and ALA doses. PAA-SPIONs and a laser together inhibited the biofilms of *P. aeruginosa* with 3 to 11-log reductions with increasing laser wavelengths. The reduction of the biofilm with ALA/PAA-SPIONs and a laser reaches 8-log for 640 nm and 13-log for 808 nm excitation. We accurately model the wavelength, time, and nanoparticle concentration dependence of PTT for the first time. These results pave the way for effective PDT/PTT elimination of biofilms of *P. aeruginosa* and *S. epidermidis*.

Received 15th September 2024,
Accepted 30th April 2025

DOI: 10.1039/d4nr03798g

rsc.li/nanoscale

Introduction

Multidrug resistance (MDR) to current antibiotics is a global threat and causes ineffective treatment of bacterial infections.[1] The World Health Organization has identified antimicrobial resistance (AMR) as "one of the top global public health and development threats". According to a Lancet report, in 2019, 1.27 million deaths worldwide were caused by AMR and another 4.95 million deaths were related to AMR.[2] A significant impact on the global economy is also predicted by the World Bank with an estimated $1 trillion in healthcare costs by 2050 and a $1–3.4 trillion loss in gross domestic product by 2030.[3] Hence, eliminating MDR bacterial infections with effective treatment techniques and drugs is of utmost importance. Besides, although MDR affects all countries, low- and middle-income countries are affected the most. Therefore, low-cost treatments and ease of access to them are equally important. One of the main causes of AMR is the formation of biofilms,

[a]*Koç University, Graduate School of Sciences and Engineering, Materials Science and Engineering, Rumelifeneri Yolu, 34450 Sariyer, Istanbul, Türkiye. E-mail: fyagci@ku.edu.tr, monbasli@ku.edu.tr*
[b]*Istanbul Technical University, Faculty of Chemical and Metallurgical Engineering, Metallurgical and Materials Engineering Department, 34469 Maslak, Istanbul, Türkiye*
[c]*Koç University Department of Electrical-Electronics Engineering, Rumelifeneri Yolu, Sariyer 34450, Istanbul, Türkiye*
[d]*School of Medicine, Medical Microbiology, Koç University, Istanbul, Türkiye*
[e]*Koç University-İşbank Center for Infectious Diseases (KUISCID), Istanbul, Türkiye*
[f]*Koc University, Department of Physics, Rumelifeneri Yolu, Sariyer 34450, Istanbul, Türkiye*
[g]*Koç University, Surface Science and Technology Center (KUYTAM), Rumelifeneri Yolu, Sariyer, 34450 Istanbul, Türkiye*
[h]*Koç University, Department of Chemistry, Rumelifeneri Yolu, Sariyer, 34450 Istanbul, Türkiye*

†Electronic supplementary information (ESI) available. See DOI: https://doi.org/10.1039/d4nr03798g

‡Equal contributions.

which are defined as thick (a few tens of microns) assemblages of microbial cells, mineral crystals, corrosion particles, clay or silt particles, or blood components in a matrix of polysaccharide materials. They can form on various surfaces, including living tissues, indwelling medical devices, industrial or potable water system piping, or natural aquatic systems or in planktonic (freely suspended) forms.[4] Due to the complex composition and structure of the biofilm matrix, antibiotics cannot easily penetrate the biofilm, and elevated doses of antibiotics are required for bacterial eradication, triggering AMR. *Pseudomonas aeruginosa* and *Staphylococcus epidermidis* are two biofilm-forming bacteria, which are highly associated with medical implant-related or wound infections with limited therapeutic options. Treatment failure for *S. epidermidis* and *P. aeruginosa* was previously reported as 31.4% and 20.6%, respectively.[5,6] Biofilms, therefore, significantly diminish the efficacy of antibiotics and increase the risk of treatment failure.[7,8] New therapeutic alternatives are essential for eliminating antibiotic-resistant bacterial infections and biofilms.

Light-based therapies, such as photothermal therapy (PTT) and photodynamic therapy (PDT), are promising techniques.[9–15] Antimicrobial PDT (aPDT) is a treatment technique for killing bacterial cells by generating light-induced phototoxicity *via* the production of reactive oxygen species (ROS), which damages the biofilm matrix.[16] In aPDT, a photosensitizer is applied to a biofilm and irradiated with a focused light source at a specific wavelength.[17,18] PTT eliminates bacterial cells by creating a local temperature increase *via* the irradiation of a photosensitizer. Inorganic nanoparticles have emerged as promising PTT photosensitizers active in NIR wavelengths, providing deeper penetration.[19,20] Superparamagnetic iron oxide nanoparticles (SPIONs) are one of the most attractive ones due to their effective light-to-heat conversion, biocompatibility, and the presence of several FDA-approved compositions.[21] SPIONs may deliver small organic photosensitizers to induce a PTT–PDT combination, which is a highly promising avenue in the treatment of bacterial infections and biofilms.[22]

In the literature, several studies have utilized combined PTT and PDT with nanoparticles to eliminate various types of bacteria. For example, a hybrid microcapsule-containing Fe_3O_4-Au-PDA/ZnPc (tetracarboxyzinc phthalocyanine) was developed for sterilization against *E. coli*. Almost all *Escherichia coli* (*E. coli*) bacteria were killed due to combined PTT/PDT at 150 μg mL^{-1} under 808 nm laser irradiation at 2 W cm^{-2} for 5 min.[23] Graphene oxide modified with tobramycin and copper sulphide nanoparticles (GO-Tob@CuS) was studied against *S. aureus* and *P. aeruginosa* under 980 nm laser irradiation at 1.5 W cm^{-2}.[24] The PTT/PDT combination killed nearly 100% of planktonic cells and provided almost 70% eradication of biofilms. It also ablated bacteria on the wound model of the dorsal skin of rats effectively. In our previous work, we showed the combined PTT–PDT potential of indocyanine green-loaded (ICG) 3-aminopropylsilane-coated superparamagnetic iron oxide nanoparticles (APTMS@SPIONs) on planktonic cells and biofilms of Gram-negative (*E. coli*, *K. pneumoniae*, and *P. aeruginosa*) and Gram-positive (*S. epidermidis*) bacteria by employing irradiation with a single 808 nm laser for 10 minutes at 1150 mW.[22] The ICG-APTMS@SPION/laser provided complete killing of all planktonic cells. Overall, 3.3-log to 4.4-log reductions were observed after laser treatment of ICG-APTMS@SPION-treated biofilms. More importantly, combined antimicrobial PTT/PDT (ICG-APTMS@SPION/laser) provided a 6.5-log reduction, which is the highest reduction value reported to date in the current literature for *K. pneumoniae* biofilms.

Here, the ALA-based aPDT and SPION-based mild PTT combination was investigated as an effective antimicrobial phototherapy approach. 4-Aminolevulinic acid (ALA) is an effective pro-drug that gets converted to the photosensitizer protoporphyrin IX (PpIX) upon cellular internalization and produces ROS when irradiated with visible wavelength lasers or LEDs (400 and 640 nm) to induce cell death.[25–29] Hence, the use of ALA provides selectivity in a way since normal cells are less efficient in converting ALA to PpIX. Besides, the red luminescence of PpIX may provide the ability to track the time for irradiation and highlight areas rich in the photosensitizer to be irradiated. The antibacterial activity of free ALA, PAA@SPIONs and ALA-loaded PAA@SPIONs (ALA/PAA@SPIONs) on planktonic cells and biofilms of Gram-negative (*Pseudomonas aeruginosa*) and Gram-positive (*Staphylococcus epidermidis*) bacteria was studied with and without laser irradiation for comparison. These bacteria are chosen since they are highly associated with biofilm-related infections, especially in hospitals. 640 nm and 808 nm diode lasers were used to achieve long-wavelength monotherapies, aPDT and aPTT, respectively, and combination therapy (640 + 808 nm co-irradiation) using ALA/PAA-SPIONs. The best results were observed with ALA/PAA-SPIONs under 640 + 808 nm laser co-irradiation. Our model results provided accurate quantitative estimations of the concentration and laser duration dependence of photothermal effects.

Materials and methods

Materials

All chemicals were of analytical grade or the highest purity. Iron(II) chloride, iron(III) chloride, Suprapur nitric acid (65%) and Suprapur sulphuric acid (96%) were purchased from Merck (purity levels 99%, Darmstadt, Germany). Poly(acrylic acid) (*M*w 2100 kDa) and dimethyl sulfoxide (Hybri-Max™) were obtained from Sigma (MO, USA). 5-Aminolevulinic acid hydrochloride (ALA) was purchased from Research Products International (RPI, USA). Vivaspin 20 centrifugal filters (5 kDa MW cut-off) were obtained from Sartorius (Goettingen, Germany). Roswell Park Memorial Institute 1640 medium (RPMI 1640, 1×), trypsin-EDTA and penicillin–streptomycin solutions were obtained from Multicell, Wisent Inc. (QC, Canada). Fetal bovine serum (FBS) was provided by Capricorn Scientific GmbH (Ebsdorfergrund, Germany). Phosphate-buffered saline (PBS) tablets and thiazolyl blue tetrazolium

bromide (MTT) were obtained from Biomatik Corp. (ON, Canada). 96-well plates were obtained from Nest Biotechnology Co., Ltd (Wuxi, China). In all experiments, only ultra-pure water was used (18.2 MΩ, RephiLe Bioscience and Technology, Shanghai, China). An L929 cell line was a gift from Prof. Engin Ulukaya (İstinye University).

Synthesis of superparamagnetic iron oxide nanoparticles

Polyacrylic acid-coated SPIONs (PAA-SPIONs) were synthesized using the co-precipitation method, based on our previous reports.[21,30] Briefly, iron salts ($[Fe^{3+}]:[Fe^{2+}] = 2:1$) and PAA (1.2 g) were dissolved in deoxygenated water under Ar flow and heated to 85 °C, and then NH_4OH (9.26 mL of 4.5 M) was injected into the solution. After 1 h of stirring under Ar at this temperature, the solution was cooled to room temperature and placed on a magnet overnight to remove any precipitated particles. Finally, PAA-SPIONs were washed several times with DI water using centrifugal filters (5 kDa) and stored at room temperature.

ALA loading onto SPIONs

ALA at a concentration of 7 mg mL^{-1} was added dropwise to the PAA-SPION solution (39.4 mg mL^{-1}) and mixed at 750 rpm for 2 h at room temperature and at pH 3. Electrostatic loading was confirmed with isothermal titration calorimetry (Affinity ITC, USA). PAA-SPIONs (1 mL, 1 mg mL^{-1} in water) were titrated with ALA (total of 250 μg mL^{-1} from 5 mg mL^{-1} in water) at a rate of 5 μg L^{-1} s^{-1} at 25 °C. Strong binding exotherms observed throughout the titration confirmed successful binding of ALA to PAA-SPIONs (ESI Fig. S1†).

Characterization

A Shimadzu UV-VIS-NIR spectrophotometer was used for obtaining absorption spectra. The hydrodynamic sizes and surface charges of nanoparticles were determined using a Malvern Zetasizer, NanoZS. An inductively coupled plasma-mass spectrometer (Agilent 7700X ICP-MS) was used to determine the iron content of nanoparticles. Samples were etched with nitric acid (65%) and sulphuric acid (96%) for the ICP-MS measurements.

Laser irradiation of aqueous solutions

The temperature increases of aqueous solutions of PAA-SPIONs were measured at 200, 600 and 1000 μg mL^{-1} Fe concentrations using 640 nm diode-laser irradiation (200 mW) for 20 minutes. The time-dependent temperature profiles of 750 μl samples were measured with a thermocouple. The steady-state maximum temperature of the cuvette–solution system was measured with a FLIR thermal camera. The intrinsic light-to-heat conversion efficiency η_i of the nanoparticles was determined according to the procedure described by Sennaroglu *et al.*,[31] by using the following relation:

$$\eta_i = \frac{(m_c c_c + m_s c_s)}{\tau_h P_i (1 - R - T)} [(T_{max} - T_0) - (T_s - T_0)].$$

Above, m_c and m_s are the masses of the cuvette and the nanoparticle solution with respective specific heat capacities c_c and c_s, P_i is the incident laser power on the cuvette, and R and T are the measured power reflection and power transmission coefficients for the cuvette–solution system. In addition, $(T_{max} - T_0)$ is the measured maximum temperature rise of the solution containing nanoparticles and $(T_s - T_0)$ is the maximum temperature rise of the pure solution (DI water in the experiments) without nanoparticles. As discussed further in ref. 31, for each heating experiment, the characteristic heating time τ_h was obtained by employing a least-squares fit to the measured time-dependent temperature rise $T(t)$ of the cuvette–solution system by using the theoretically expected temporal variation given by

$$T(t) = T_{max} + (T_0 - T_{max}) \exp\left(-\frac{t}{\tau_h}\right).$$

Modelling temperature dynamics in photothermal therapy

For modelling the photothermal heating and cooling dynamics, we developed an analytical model and two computational models. The analytical model captures heating and cooling by accounting for the detailed energy balance of incoming laser energy consistent with and extending our earlier work,[22] heating of nanoparticles and thermal dissipation of the system. We used spectroscopic ellipsometry to fit Ψ and Δ of the nanoparticles to obtain their refractive index and extinction coefficients over the visible and near-infrared wavelengths. The analytical model starts with the following equation:

$$dQ_{injected} = dQ_{dissipated} + m_{PAA\text{-}SPION} C_{PAA\text{-}SPION} dT + m_{water} C_{water} dT$$

Here, the injected heat from the laser is proportional to the laser power density (I, W m^{-2}), duration (t) and absorption (A). Thus, the energy fluence (F, J m^{-2}) of laser excitation at a given wavelength is given by F(J m^{-2}) = $A \times I \times t$. The injected heat is then found by multiplying the energy fluence with the illuminated volume V. Since the thermal simulations are conducted in a volumetric bath, the laser energy is given in terms of J cm^{-3} for a given unit volume of photonic simulation using Beer's law:

$$dQ_{injected} = E_{density} \times \text{illuminated surface area} \times \text{thickness}$$

We assumed that the laser is uniformly absorbed by the medium, although this might differ in *in vivo* experiments.

As the medium heats with the absorbed laser energy, the radiative and convective dissipation terms must be considered to account for the thermal dynamics of the experiments: dQdissipated = dQradiation + dQconvection. For simplicity, the detailed expressions and parameters used for these terms are presented in the ESI.† For calculating Qdissipated and heat transfer, we used ANSYS Lumerical Heat Solver software. Finally, the temperature change dynamics is found using $Q = mC\Delta T$ for a given solution mass (m) and specific heat (C) with a dissipation term dominated by the medium mass ($m$water ≫ mPAA-SPION):

$$\Delta T = \frac{dQ_{injected} - dQ_{dissipated}}{m_{PAA\text{-}SPION} C_{PAA\text{-}SPION} + m_{water} C_{water}} \approx \frac{Q_{injected} - Q_{dissipated}}{m_{water} C_{water}}$$

This approach successfully captures the increasing dissipation rate of the heated medium and nanoparticles. The increasing dissipation rate is responsible for the temperature equilibrium observed in the experiments, as shown in Fig. 1.

For simulating the light-to-heat conversion of nanoparticles, we created photonic and thermal simulation setups using ANSYS Lumerical software. First, we used the ANSYS Lumerical FDTD Solver and parameterized the periodic cubic unit cell volume of the given simulation to mimic different concentrations of the solution. Thickness is defined by the single side length of the unit cells. Each unit cell contains one particle, and these unit cells repeat periodically to form a thin film. The dimensions of the cubic unit cells corresponding to different concentrations of nanoparticles and their calculation details are presented in the ESI.†

If the concentration of the solution is very high such that the volume fraction of nanoparticles is comparable to the medium volume, the FDTD solution might not be sufficient due to scattering and plasmonic effects in a periodic structure. To validate the FDTD simulation, we set up a second simulation using Effective Medium Theory and the ANSYS Lumerical Stack Solver for creating a homogeneous effective medium.

In our periodic FDTD simulations, we defined a cubic unit cell for each particle. The relationship between the number of particles, volume and concentration was determined based on the following formula:

$$V_{\text{unit cell}} = W_{\text{molecular}}/(CN)$$

for each particle, where W, C, and N are the nanoparticle molecular mass, nanoparticle concentration and Avagadro's number, respectively.

Cell culture

Healthy mouse fibroblast L929 cells were grown at 37 °C in a 5% CO_2 humidified incubator in DMEM medium supplemented with 10% fetal bovine serum and 1% streptomycin.

Dark toxicity

The dose-dependent toxicity of free ALA, PAA-SPIONs and ALA/PAA-SPIONs was investigated in L929 cells between 21 and 336 μg ALA per mL or between 37.5 and 600 μg Fe per mL using the standard MTT assay. Cells were seeded at a density of 1×10^4 cells per well into 96-well plates and incubated for 24 h. Cells were incubated with free ALA, SPIONs and ALA-SPIONs in fresh culture medium for 24 h, and then the medium was replaced with 50 μg mL^{-1} MTT solution (5 mg mL^{-1} in PBS) and 150 μg mL^{-1} fresh medium. After a 4 h incubation, DMSO : ethanol (1 : 1 v/v) was added to dissolve the purple formazan crystals formed by viable cells. Absorbance was recorded using a microplate reader (Synergy H1 Biotek Instruments) at 600 nm with a reference reading at 630 nm. The following formula was used to calculate relative cell viability:

$$\text{Cell viability } (\%) = [\text{absorbance sample}/\text{absorbance control}] \times 100 \ (n = 3)$$

Bacterial isolates

Pseudomonas aeruginosa ATCC® 700829™ and *Staphylococcus epidermidis* ATCC®35984™ were used in the experiments.

Antibacterial activity on planktonic bacteria

A single colony of bacteria from overnight cultures was inoculated into Tryptic Soy Broth (TSB, BD™ Bacto™) and incubated overnight at 37 °C at 135 rpm. ALA, PAA-SPIONs and ALA/PAA-SPIONs were added to the cell suspension at final concentrations of 0.5 mM ALA per 150 μg Fe per mL and 2 mM ALA per 600 μg Fe per mL. TSB was added for the control group. Cultures were incubated at 37 °C overnight. The survival of bacteria was determined by colony counting after serial tenfold dilutions. At least a 2-log (99%) growth reduction in mean CFU per mL values is considered a significant inhibition. All studies were performed three times to ensure reproducibility.

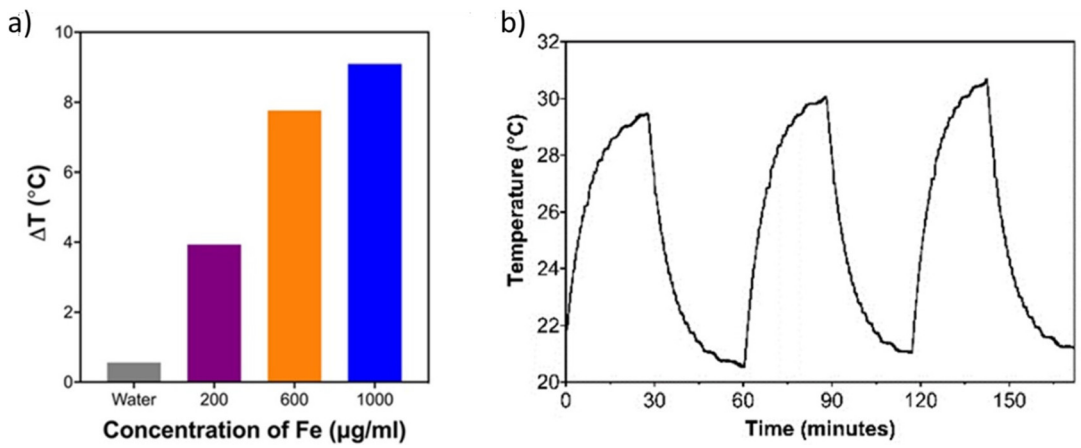

Fig. 1 (a) Time-dependent change in the temperature of PAA-SPION solutions and DI water irradiated at 640 nm (200 mW) for 20 min at different Fe concentrations and (b) temperature of the PAA-SPION solution (1000 μg Fe per mL) during the laser on/off cycles.

Anti-biofilm activity

Biofilms were produced in 96-well plates with a protocol described by Merritt *et al.*[32] Then, media were gently removed from the wells, and fresh TSB-glucose (control) or ALA, PAA-SPIONs and ALA/PAA-SPIONs were added into wells at 2 mM ALA per 600 μg Fe per mL dose. After overnight incubation at 37 °C, the survival of bacteria was determined by colony counting as described above, following homogenization of the biofilm. At least a 2-log growth reduction in mean CFU per mL values was considered significant inhibition. All studies were performed in three replicates.

Laser irradiation of planktonic cells and biofilms

Monotherapies for both planktonic bacteria and biofilms were performed with 10 min of irradiation from the bottom of the plates at 640 nm (0.75 W cm^{-2}) and 808 nm (2.6 W cm^{-2}) using diode lasers. Co-irradiation was performed in the same way using 640 + 808 nm diode lasers (0.75 + 2.6 W cm^{-2}) for 10 minutes. After laser treatment, planktonic cells and biofilms were incubated overnight at 37 °C, and the survival of both planktonic and biofilm cells was determined by using the protocol described above.

PpIX detection

Qualitative analysis. *In vitro* imaging of biofilms was performed using a LEICA live cell microscope at 20× magnification. Biofilms were fixed with 3.5% formaldehyde and mounted with DAPI (mounting medium with DAPI – aqueous, Fluoroshield (ab104139)). PpIX luminescence was observed at 630 nm with 590 nm excitation.

Quantitative analysis. Planktonic bacteria were cultured and treated overnight with free ALA, PAA-SPION, and ALA/PAA-SPION. Each well's fluorescence was measured at 635 nm using a Synergy H1 microplate reader (Biotek) after overnight incubation at 37 °C. The control group consisted of untreated cells.

Quantification of nanoparticle uptake

Internalization of nanoparticles was determined by a quantitative method based on the Fe content measured by ICP-MS. Biofilms were treated with PAA-SPIONs and ALA/PAA-SPIONs at 600 μg Fe per mL with the above-mentioned protocol. To remove free nanoparticles, biofilms were washed with PBS and collected into flasks. All liquid media were removed by gentle heating. Following the heating step, 1 mL of a H_2SO_4 : HNO_3 (1 : 9) mixture was added to the flasks, and the flasks were kept for 1 week for digestion. Then, Fe content was determined by ICP-MS. All samples were prepared in three replicates. Non-treated biofilms were included as the control group.

Statistical analysis

The Kruskal–Wallis test was performed for statistical analysis using GraphPad Prism 9.0 software. All treated groups were independently compared to their untreated control group for each corresponding set of planktonic or biofilm experiments. The difference was considered statistically significant for $p < 0.05$.

Results and discussion

Synthesis and characterization of nanoparticles

Initially, colloidally stable, aqueous PAA-SPIONs were produced with small hydrodynamic sizes (number-based hydrodynamic size of 12.4 nm) with a negative surface charge (−15.6 mV) by a co-precipitation method based on our previous reports.[21,30] Then, zwitterionic ALA was loaded onto the PAA-SPIONs *via* electrostatic interaction, which was confirmed by isothermal titration calorimetry (Fig. S1†). After ALA loading, there was no significant change in the hydrodynamic size, while the ζ potential was slightly reduced to −22.5 mV. Therefore, ALA/PAA-SPIONs were successfully developed for dual antibacterial PTT and PDT.

Laser-induced temperature increase in aqueous colloidal solutions of nanoparticles

The photothermal heating potential of PAA-SPION was assessed under 640 nm laser irradiation at 200 mW for 20 min as a function of nanoparticle concentration. Irradiation of DI water (control) did not cause any changes in temperature, indicating that the source of temperature increase was the SPIONs. ΔT of PAA-SPION was 3.9, 7.8, and 9.1 °C at Fe concentrations of 200, 600 and 1000 μg mL^{-1} (Fig. 1a). Three cycles of laser on/off experiments showed no loss in heating potential with a ΔT of 9.4 °C in every cycle, indicating the high photothermal stability of PAA-SPIONs (Fig. 1b). The photothermal conversion efficiency of PAA-SPION was calculated as 89.7% based on the method detailed in the literature.[31] Overall, these results showed that PAA-SPION can be used as a highly stable and efficient PTT agent.

Detailed modelling of photothermal effects

Fig. 2a shows the normalized absorption spectra for different concentrations of nanoparticles in the visible and near-infrared wavelengths, calculated using both FDTD and effective medium theory. The extinction coefficients of the nanoparticles decrease at longer wavelengths, and hence, the normalized absorption also decreases at longer wavelengths. The FDTD and the analytical effective medium theory solutions are consistent, and they validate each other. We used consistent notation with our earlier model,[31] which captured the convective and radiative heat transfer of Ag_2S–glutathione quantum dots. That study[31] focused on the photothermal conversion efficiency calculations for quantum dots excited with a Ti^{3+}: sapphire laser. Since the particle volume to host material volume ratio in solution is small, periodic unit cells do not couple with each other. The FDTD solution shows that the absorption is essentially due to the high refractive index of the nanoparticles, and the contribution from scattering is negligible. Fig. 2b shows one heating–cooling cycle as a result of a laser on/off cycle at a 640 nm excitation wavelength for 5, 10,

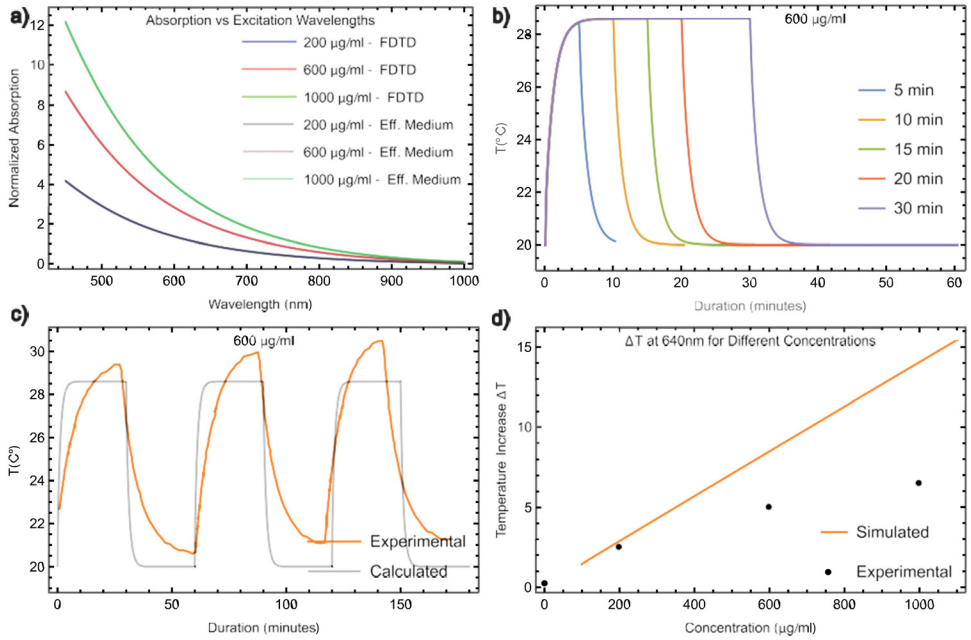

Fig. 2 Results of modelling temperature dynamics in photothermal therapy. (a) Calculated absorption values of aqueous PAA-SPIONs at 200, 600, and 1000 µg mL^{-1} Fe concentrations for FDTD simulations and effective medium theory. (b) Calculated 1 cycle of laser on/off (heating–cooling) for 5, 10, 15, 20, and 30 min laser pulses. (c) Comparison of experimental and calculated heating–cooling cycles for aqueous PAA-SPIONs at 600 µg mL^{-1} Fe concentration for a 30 min laser pulse. (d) Steady-state comparison of experimental and simulated temperature increases of aqueous PAA-SPIONs at different concentrations. As a result of this modelling study, we focus on 200 and 600 µg mL^{-1} Fe concentrations in antibacterial experiments and did not use 1000 µg mL^{-1} Fe since nonlinear optical interactions at this concentration such as increased optical scattering and reflection might start becoming more prominent.

15, 20 and 30 min long laser pulses. These model results are quantitatively consistent with the experimental observations shown in Fig. 1. Fig. 2c shows that the analytical and numerical models capture the reversible heating–cooling cycle for the nanoparticles, which are also observed experimentally. Finally, Fig. 2d shows the steady-state temperature increase for experimental and numerical model results. The model captures the increasing heating effectiveness with higher nanoparticle concentrations. The model is quantitatively close to the experimentally observed temperature changes as shown in Table 1. The slight differences can be attributed to experimental nanoparticle inhomogeneities and slight differences in concentrations.

Dark toxicity of free ALA, PAA-SPIONs and ALA/PAA-SPIONs

The dose-dependent cytotoxicity of free ALA, PAA-SPIONs and ALA/PAA-SPIONs was first evaluated on a healthy cell line (L929) at different concentrations (21–336 µg ALA per mL or 37.5–600 µg Fe per mL) using a standard MTT assay after 24 h of incubation. No significant toxicity was detected in the studied concentration range (ESI Fig. S2†), confirming that free ALA, PAA-SPIONs and ALA/PAA-SPIONs do not induce toxicity when not irradiated with lasers.

Cellular uptake

The quantitative uptake of PAA-SPIONs and ALA/PAA-SPIONs by the biofilms was determined from the Fe content of the treated biofilms by ICP-MS (Fig. 3a). Both *P. aeruginosa and S. epidermidis* were treated with PAA-SPIONs and ALA/PAA-SPIONs at 600 µg Fe per mL for 24 h before the analysis. The internalization of PAA-SPIONs and ALA/PAA-SPIONs by *P. aeruginosa* was about 3%. *S. epidermidis* internalized more nanoparticles (NPs) than *P. aeruginosa* which is 50% for PAA-SPIONs and 43% for ALA/PAA-SPIONs. These results

Table 1 Absorption and temperature increase

Nanoparticle concentration (µg mL^{-1} Fe)	Absorption ratio (FDTD)	Absorption ratio (effective volume)	Normalized absorption	Estimated temperature increase (°C)	Experimental temperature increase (°C)
Water	—	—	—	—	0.25
200	0.96747×10^{-5}	0.94676×10^{-5}	1	2.8	3.9
600	2.01276×10^{-5}	1.96928×10^{-5}	2.08	8.5	7.8
1000	2.82889×10^{-5}	2.76818×10^{-5}	2.92	14	9.1

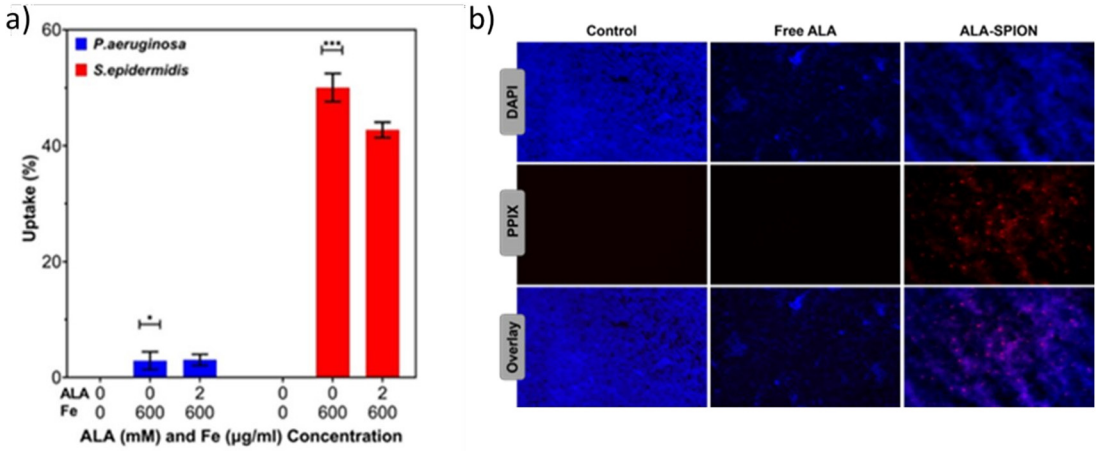

Fig. 3 (a) Uptake of PAA-SPIONs and ALA/PAA-SPIONs by *P. aeruginosa and S. epidermidis* biofilms treated at a 600 μg Fe per mL concentration based on ICP analysis. (b) Fluorescence microscopy images of *P. aeruginosa* biofilms treated with free ALA (0.5 mM) or ALA/PAA-SPIONs (150 μg Fe per mL). Images were taken with the DAPI filter (Ex: 365, Em: 465), the Alexa 610 filter for the detection of PpIX luminescence (Ex: 590, Em: 630), and at 20× magnification.

showed that a high number of NPs can be internalized by *S. epidermidis* due to its positively charged nature.

Enhanced uptake of ALA/PAA-SPIONs compared to free ALA was confirmed qualitatively by the red fluorescence of intracellular PpIX (Fig. 3b). No PpIX emission was observed in biofilms treated with free ALA, while ALA/PAA-SPION treatment resulted in strong PpIX emission. These microscopy images also showed the ability of optical detection of ALA/PAA-SPIONs, which allows image-guided selection of the area for irradiation.

Although the internalization was higher in *S. epidermidis*, it did not totally reflect the antibacterial and anti-biofilm activity which, overall, was higher in *P. aeruginosa* (Fig. 4–7). Adsorption of nanoparticles onto the cell wall leads to cell wall depolarization and disintegration, which alters the negative charge of the cell wall to become more permeable.[33] However, along with the cell wall structural differences, cellular factors such as endogenous porphyrins present in *P. aeruginosa* might also be triggered during laser irradiation to cause extended bacterial inhibition indirectly.[34,35] Furthermore, *S. epidermidis* is known to be more resistant to light irradiation and heat.[36,37]

Antibacterial activity on planktonic cells

The dose-dependence of growth inhibition of free ALA, PAA-SPIONs and ALA/PAA-SPIONs was evaluated with and without laser irradiation at 150 and 600 μg Fe per mL or 0.5- and 2 mM ALA concentrations on planktonic cells of *P. aeruginosa* and *S. epidermidis.* Laser irradiation was per-

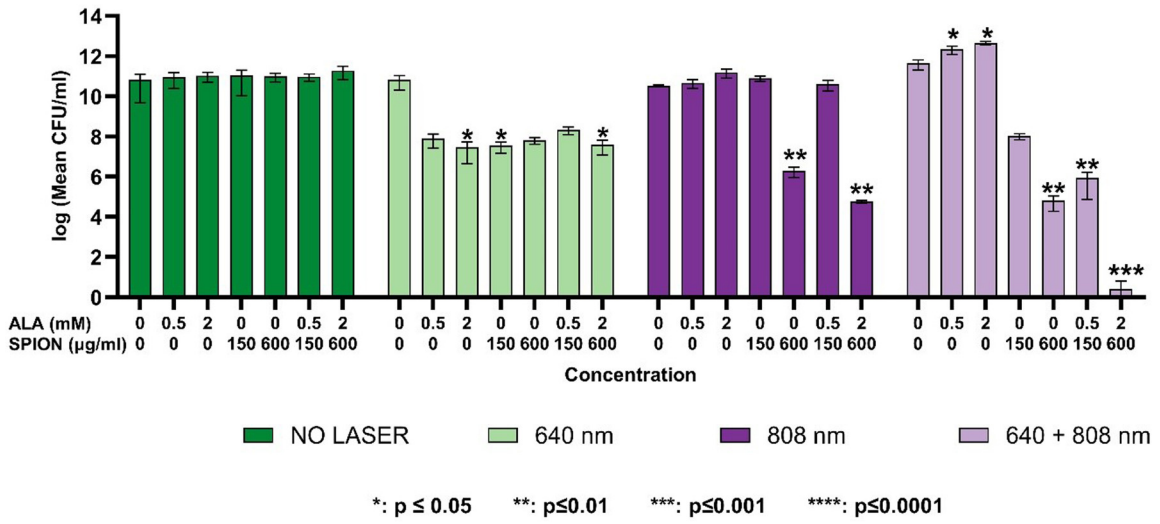

Fig. 4 Measured effect of free ALA, SPIONs and ALA-SPIONs on the inhibition of *P. aeruginosa* planktonic cells with and without laser irradiation. Control: untreated or only laser-treated planktonic cells. All laser experiments were performed under 640 nm, 808 nm and dual laser irradiation (640 + 808 nm) at 0.75 W cm^{-2}, 2.6 W cm^{-2} and 0.75 + 2.6 W cm^{-2} for 10 minutes, respectively.

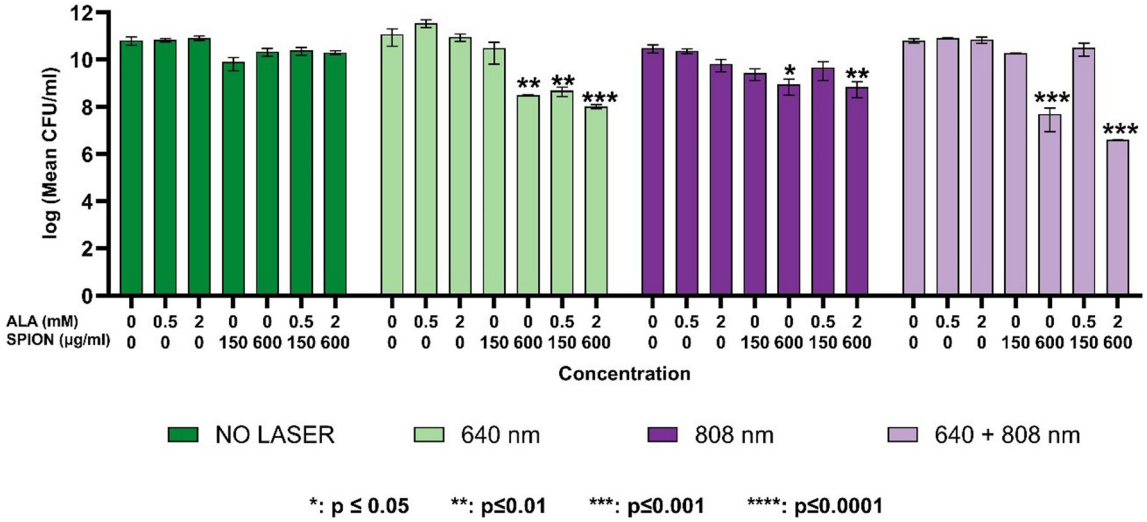

Fig. 5 Measured effect of free ALA, SPIONs and ALA-SPIONs on the inhibition of *S. epidermidis* planktonic cells with and without laser irradiation. Control: untreated or only laser-treated planktonic cells. All laser experiments were performed under 640 nm, 808 nm and dual laser irradiation (640 + 808 nm) at 0.75 W cm^{-2}, 2.6 W cm^{-2} and 0.75 + 2.6 W cm^{-2} for 10 minutes, respectively.

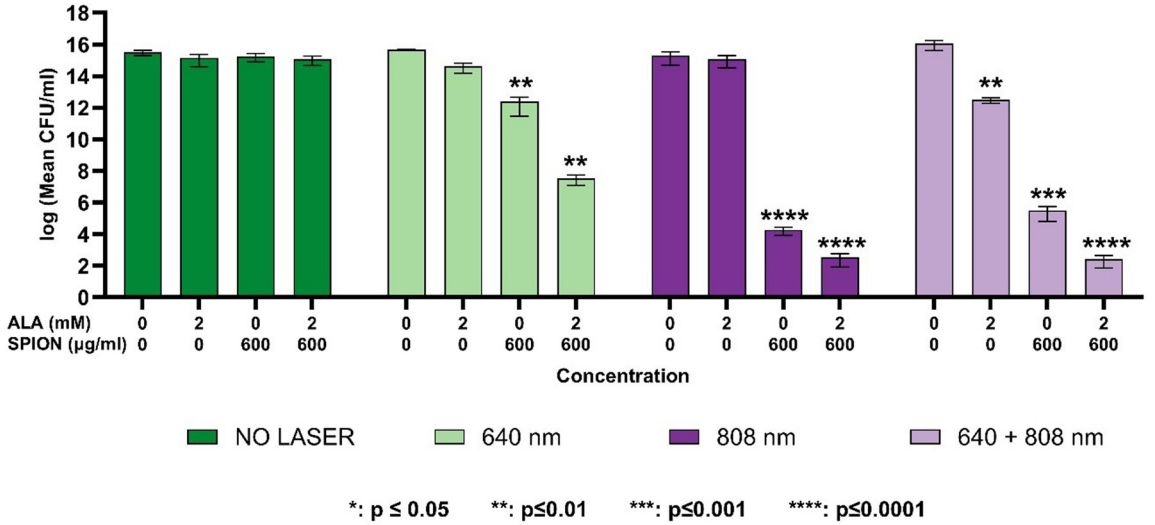

Fig. 6 Measured effect of free ALA, SPIONs and ALA-SPIONs on the inhibition of *P. aeruginosa* biofilms with and without laser irradiation. Control: untreated or only laser-treated biofilms. All laser experiments were performed under 640 nm, 808 nm and dual laser irradiation (640 + 808 nm) at 0.75 W cm^{-2}, 2.6 W cm^{-2} and 0.75 + 2.6 W cm^{-2} for 10 minutes, respectively.

formed at 640 nm (0.75 W cm^{-2}), 808 nm (2.6 W cm^{-2}) and 640 + 808 nm (0.75 + 2.6 W cm^{-2}) for 10 min on both bacterial types. In the absence of laser irradiation, there was no growth inhibition in the planktonic cells of either bacterium treated with any of the free ALA, PAA-SPIONs, or ALA/PAA-SPIONs. Growth reduction of planktonic cells was studied at two concentrations: nanoparticles at 150 and 600 μg mL^{-1} Fe concentrations and 0.5 and 2 mM ALA.

Inhibition of *P. aeruginosa* planktonic cell growth. Against planktonic cells of *P. aeruginosa*, both low and high doses of free ALA caused a 3-log growth reduction under 640 nm irradiation (with mean CFU per mL values of 8.07×10^7, $p > 0.05$ and 2.96×10^7, $p = 0.0239$, respectively), while there was no growth reduction under 808 nm or 640 + 808 nm co-irradiation (Fig. 4). At 150 μg Fe per mL, PAA-SPIONs did not cause a significant growth reduction at 808 nm; however, they caused a 2-log reduction under 640 + 808 nm co-irradiation (a mean CFU per mL of 1.06×10^8) and a 3-log reduction under 640 nm irradiation (a mean CFU per mL of 3.45×10^7, $p = 0.0283$). A higher growth reduction was observed with increasing concentration to 600 μg Fe per mL; 3-log at 640 nm (a mean CFU per mL of 6.55×10^7), 4-log under 808 nm (a mean CFU per mL of 1.99×10^6, $p = 0.0061$) and 6-log at 640 + 808 nm (a mean CFU per mL of 6.48×10^4, $p = 0.0015$)

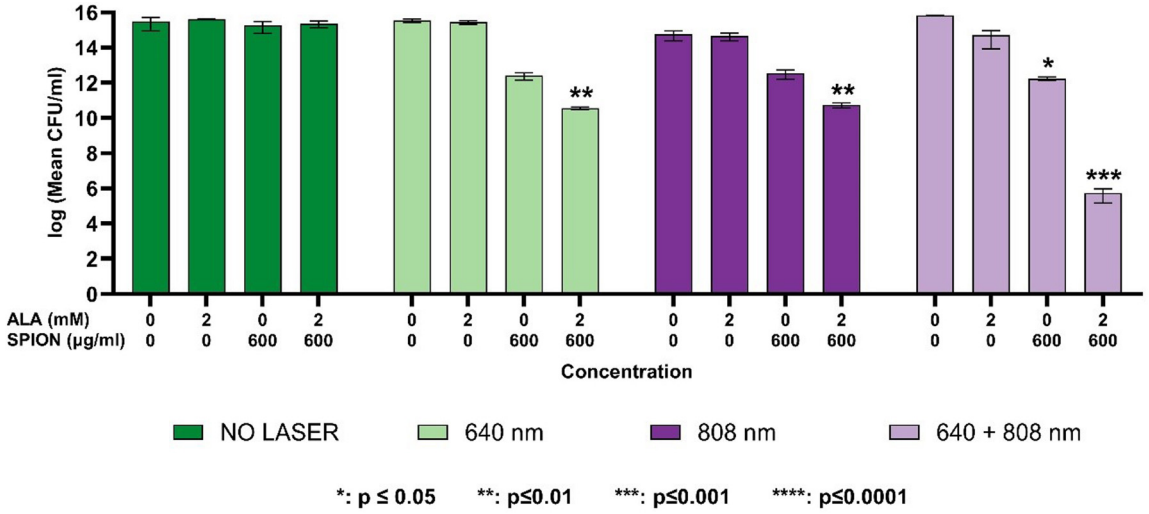

Fig. 7 Measured effect of free ALA, SPIONs and ALA-SPIONs on the inhibition of *S. epidermidis* biofilms with and without laser irradiation. Control: untreated or only laser-treated biofilms. All laser experiments were performed under 640 nm, 808 nm and dual laser irradiation (640 + 808 nm) at 0.75 W cm^{-2}, 2.6 W cm^{-2} and 0.75 + 2.6 W cm^{-2} for 10 minutes, respectively.

irradiation (Fig. 4). ALA/PAA-SPIONs, respectively, exhibited 2-log (a mean CFU per mL of 2.15×10^8) and 5-log growth reductions (a mean CFU per mL of 8.78×10^5, $p = 0.0034$) under 640 and 640 + 808 nm irradiation (mean CFU per mL and p), at 0.5 mM ALA and 150 μg Fe per mL dose. There was no significant inhibition at 808 nm single wavelength irradiation at the same dose. ALA/PAA-SPIONs showed a dramatic effect on growth reduction at 600 μg Fe per mL and a 2 mM ALA dose. Almost total eradication was achieved with the laser irradiation of ALA/PAA-SPIONs under 640 + 808 nm co-irradiation (a mean CFU per mL of 2.5×10^0, $p = 0.0004$). Although lower inhibition rates were observed with 640 and 808 nm irradiation alone, the growth inhibition rates were still significant (mean CFU per mL values of 3.93×10^7, $p = 0.0344$ and 5.72×10^4, $p = 0.0011$, respectively). The mean CFU per mL for the control group (without nanoparticles and laser irradiation) was found to be 6.48×10^{10} CFU mL^{-1} for *P. aeruginosa.*

Inhibition of *S. epidermidis* planktonic cell growth. Against planktonic cells of *S. epidermidis*, neither low nor high doses of free ALA nor 150 μg Fe per mL dose of PAA-SPIONs caused significant growth inhibition. Increasing the concentration of PAA-SPIONs to 600 μg Fe per mL caused a 2-log inhibition at 640 nm and 808 nm (a mean CFU per mL of 3.20×10^8, $p = 0.0038$ and a mean CFU per mL of 9.00×10^8, $p = 0.0242$, respectively). A higher growth reduction (3-log) was observed under 640 + 808 nm irradiation (a mean CFU per mL of 5.10×10^7, $p = 0.0004$) (Fig. 5). ALA/PAA-SPIONs exhibited significant growth reduction (2-log) only under 640 nm irradiation (a mean CFU per mL of 4.86×10^8, $p = 0.0062$), with 0.5 mM ALA and 150 μg Fe per mL dose. Growth inhibition achieved with ALA/PAA-SPIONs at 600 μg Fe per mL and a 2 mM ALA dose was 2-log for 640 nm (a mean CFU per mL of 1.07×10^8, $p = 0.0009$), 2-log for 808 nm (a mean CFU per mL of 7.00×10^8, $p = 0.0072$) and 4-log for 640 + 808 nm (a mean CFU per mL of 4.03×10^6, $p = 0.0001$) irradiation, respectively. The mean CFU per mL for the control group (without nanoparticles and laser irradiation) was found to be 6.73×10^{10} CFU per mL for *S. epidermidis.*

Anti-biofilm activity

Inhibition of *P. aeruginosa* biofilm. Against *P. aeruginosa* biofilm, a high dose of free ALA caused a significant reduction (3-log) under 640 + 808 nm irradiation (a mean CFU per mL value of 3.13×10^{12}, $p = 0.0093$), while there was no reduction under 640 or 808 nm irradiation (Fig. 6). A concentration of 600 μg Fe per mL for PAA-SPIONs caused a 3-log reduction under 640 nm (a mean CFU per mL of 2.51×10^{12}, $p = 0.0068$), an 8-log reduction at 808 nm (a mean CFU per mL of 1.83×10^4, $p < 0.0001$) and a 7-log reduction at 640 + 808 nm (a mean CFU per mL of 3.12×10^5, $p = 0.0003$) irradiation, respectively. ALA/PAA-SPIONs, on the other hand, caused an 8-log reduction under 640 nm (a mean CFU per mL of 3.27×10^7, $p = 0.0013$) and a 10-log reduction under 808 nm (a mean CFU per mL of 3.33×10^2, $p < 0.0001$) and under 640 + 808 nm irradiation (a mean CFU per mL of 2.60×10^2, $p < 0.0001$). The mean CFU per mL value for the untreated control biofilm was 3.07×10^{15}.

Inhibition of *S. epidermidis* biofilm. Against *S. epidermidis* biofilms, a high dose of free ALA did not cause a significant reduction at either of the irradiations (Fig. 7). A concentration of 600 μg Fe per mL for PAA-SPIONs caused a 3-log reduction only under 640 + 808 nm irradiation (a mean CFU per mL of 1.73×10^{12}, $p = 0.0471$). ALA/PAA-SPIONs, on the other hand, caused a 5-log reduction under 640 nm irradiation (a mean CFU per mL of 3.70×10^{10}, $p = 0.0018$) and 808 nm irradiation (a mean CFU per mL of 5.67×10^{10}, $p = 0.0065$), while the reduction was enhanced to a 10-log reduction under 640 + 808 nm irradiation (a mean CFU per mL of 5.55×10^{10}, $p = 0.0002$). The mean CFU per mL value for the untreated control biofilm was 3.07×10^{15}.

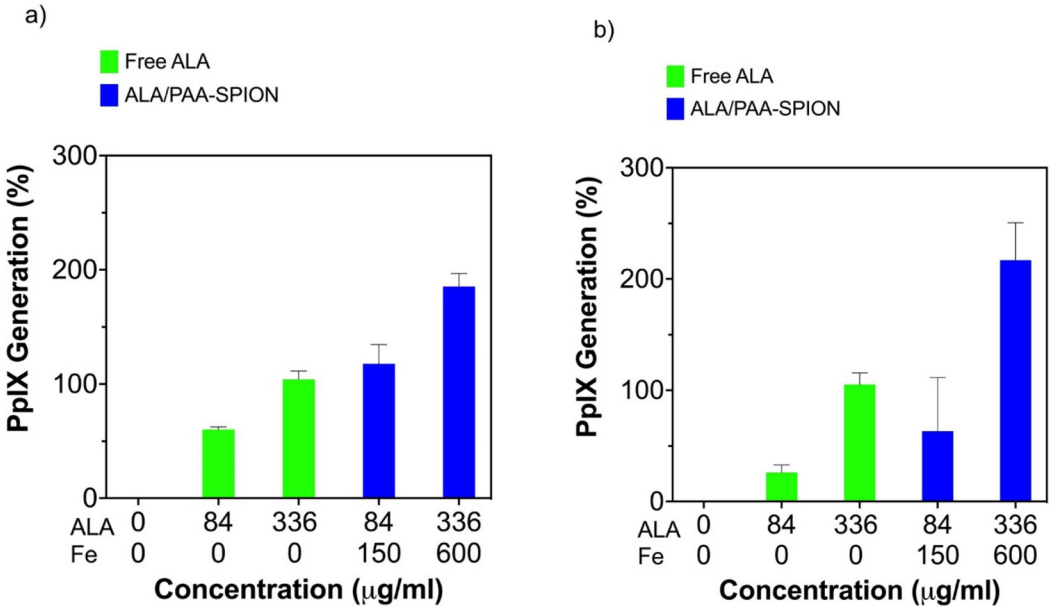

Fig. 8 (a) Intracellular formation of PpIX through administration of free ALA and ALA/PAA-SPIONs after overnightincubation in *P. aeruginosa* planktonic cells (PpIX:$\lambda_{excitation}$:405nmand $\lambda_{emission}$:635 nm). (b) Intracellular formation of PpIX through administration of free ALA and ALA/PAA-SPIONs after overnight incubation in *S. epidermidis* planktonic cells (PpIX: $\lambda_{excitation}$: 405 nm and $\lambda_{emission}$: 635 nm).

Photothermal temperature increase during laser treatment

Temperature increases during laser irradiation of *P. aeruginosa* biofilms that were treated with free ALA, PAA-SPION, and ALA/PAA-SPION at 600 μg Fe per mL and 2 mM ALA concentrations were monitored with a thermal camera. Cells without laser treatment were used as a control (ESI Fig. S3†).

In the control group, no temperature increase was observed under 640 nm irradiation, and only a 1.7 °C and 2.1 °C temperature increase was detected under 808 nm and 640 + 808 nm irradiation. The laser irradiation of biofilms treated with free ALA did not cause any temperature increase at 640 nm; however, it provided 2.2 °C and 3.6 °C temperature increases at 808 nm and 640 + 808 nm, respectively. PAA-SPIONs and ALA/PAA-SPIONs caused almost the same temperature increase in biofilms at 640 (2.5 °C) and 808 nm (8 °C) and a comparable temperature increase at 640 + 808 nm (10.2 °C for PAA-SPIONs and 9.3 °C for ALA/PAA-SPIONs).

PpIX generation

The conversion of ALA into PpIX was quantitatively measured by the fluorescence intensity of PpIX *via* its emission at 635 nm. Incubation of *P. aeruginosa* planktonic cells with 0.5 mM ALA resulted in a 60% increase in PpIX luminescence, while 2 mM ALA resulted in a 104% increase in intracellular PpIX. When 0.5 and 2 mM ALA were delivered into *P. aeruginosa* planktonic cells with PAA-SPIONs, a 117% and 185% increase in PpIX generation was observed, respectively (Fig. 8(a)). For *S. epidermidis*, incubation of planktonic cells with 0.5 mM and 2 mM ALA resulted in a 26% and 105% increase in PpIX generation inside the cells, respectively. Delivery of 0.5 mM and 2 mM ALA into *S. epidermidis* planktonic cells resulted in a 63% and 216% increase in PpIX generation, respectively (Fig. 8(b)).

Conclusion

This study successfully demonstrates the potential of ALA-loaded PAA-SPIONs as an innovative dual photothermal therapy (PTT) and photodynamic therapy (PDT) platform for the effective eradication of biofilms formed by *Pseudomonas aeruginosa* and *Staphylococcus epidermidis*. The combined PTT/PDT approach showed significant bactericidal effects, achieving up to a 13-log reduction in biofilm populations, particularly with 640 + 808 nm co-irradiation, which represents the highest level of biofilm inhibition reported to date using a nanoparticle-based dual-therapy system. In our experiments, co-irradiation was performed by using free-space beams at 640 and 808 nm for the sake of a proof-of-principle demonstration. We note that the proposed method of dual laser therapy can be easily extended to practical clinical use by coupling both laser beams into a single optical fiber, where treatment can be applied either simultaneously at both wavelengths or with one laser wavelength at a time, without the need for delicate optical alignment of the beams. We further foresee that the fast development of powerful, cost-effective lasers at multi-watt levels or higher will enable even wider use of lasers in the clinic and the ability to irradiate large-area biofilms.

This work highlights the significance of the combination of SPIONs with 4-aminolevulinic acid (ALA), enabling both photothermal and photodynamic effects while maintaining low dark toxicity in healthy cells. The efficient conversion of ALA to pro-

toporphyrin IX (PpIX) enhanced the photodynamic efficacy, while the superparamagnetic properties of SPIONs facilitated effective heat generation under near-infrared (NIR) laser irradiation. This dual-action strategy allowed for significant biofilm disruption, particularly for *P. aeruginosa*, with an 8-log reduction observed under 640 nm irradiation and a remarkable 13-log reduction under 808 nm co-irradiation.

The photothermal heating efficiency of PAA-SPIONs was thoroughly modeled, and the experimental data aligned closely with theoretical predictions, establishing a reliable foundation for predicting nanoparticle-based PTT efficacy. The developed model accurately captured the dynamics of heat generation and dissipation, emphasizing the importance of nanoparticle concentration and laser wavelength in achieving optimal therapeutic outcomes.

This study pioneers the combination of mild photothermal effects with selective photodynamic action, providing a non-invasive and antibiotic-free solution to biofilm-related infections. By precisely controlling nanoparticle concentrations and laser parameters, this approach minimizes potential side effects while maximizing therapeutic efficacy. The findings pave the way for further optimization of nanoparticle-based therapies, potentially revolutionizing the treatment of antibiotic-resistant bacterial infections. This study represents a significant step forward in developing alternative therapies to combat the global threat of antimicrobial resistance.

Author contributions

Data availability

The data supporting this article have been included as part of the ESI.†

Conflicts of interest

There are no conflicts to declare.

Acknowledgements

M. C. O., C. K. and R. Y. acknowledge support from the European Research Council (ERC) *via* the ERC Proof of Concept project SuperPHOTON (no. 101100718). K. O., M. C. O. and H. Y. A. acknowledge the Turkish Institutes of Health (TÜSEB) Group B Project funding (no. 33131).

References

1 A. Chatterjee, M. Modarai, N. R. Naylor, S. E. Boyd, R. Atun, J. Barlow, *et al.*, Quantifying drivers of antibiotic resistance in humans: a systematic review, *Lancet Infect. Dis.*, 2018, **18**(12), e368–e378.

2 Antimicrobial Resistance C, Global burden of bacterial antimicrobial resistance in 2019: a systematic analysis, *Lancet*, 2022, **399**(10325), 629–655.

3 S. Ajulo and B. Awosile, Global antimicrobial resistance and use surveillance system (GLASS 2022): Investigating the relationship between antimicrobial resistance and antimicrobial consumption data across the participating countries, *PLoS One*, 2024, **19**(2), e0297921.

4 R. M. Donlan, Biofilms: microbial life on surfaces, *Emerging Infect. Dis.*, 2002, **8**(9), 881–890.

5 N. Bagnall, S. Vig and P. Trivedi, Surgical-site infection, *Surgery*, 2009, **27**(10), 426–430.

6 M. Riool, L. de Boer, V. Jaspers, C. M. van der Loos, W. J. B. van Wamel, G. Wu, *et al.*, Staphylococcus epidermidis originating from titanium implants infects surrounding tissue and immune cells, *Acta Biomater.*, 2014, **10**(12), 5202–5212.

7 H. C. Flemming and J. Wingender, The biofilm matrix, *Nat. Rev. Microbiol.*, 2010, **8**(9), 623–633.

8 J. Iredell, J. Brown and K. Tagg, Antibiotic resistance in Enterobacteriaceae: mechanisms and clinical implications, *Br. Med. J.*, 2016, **352**, h6420.

9 V. Perez-Laguna, L. Perez-Artiaga, V. Lampaya-Perez, I. Garcia-Luque, S. Ballesta, S. Nonell, *et al.*, Bactericidal Effect of Photodynamic Therapy, Alone or in Combination with Mupirocin or Linezolid, on Staphylococcus aureus, *Front. Microbiol.*, 2017, **8**, 1002.

10 W. C. de Melo, P. Avci, M. N. de Oliveira, A. Gupta, D. Vecchio, M. Sadasivam, *et al.*, Photodynamic inactivation of biofilm: taking a lightly colored approach to stubborn infection, *Expert Rev. Anti Infect. Ther.*, 2013, **11**(7), 669–693.

11 J. W. Xu, K. Yao and Z. K. Xu, Nanomaterials with a photothermal effect for antibacterial activities: an overview, *Nanoscale*, 2019, **11**(18), 8680–8691.

12 W. Li, X. Geng, D. Liu and Z. Li, Near-Infrared Light-Enhanced Protease-Conjugated Gold Nanorods As A Photothermal Antimicrobial Agent For Elimination Of Exotoxin And Biofilms, *Int. J. Nanomed.*, 2019, **14**, 8047–8058.

13 Y. Ran, J. Shi, Y. Ding, L. Li, D. Lu, Y. Zeng, *et al.*, Black Phosphorus Nanosheets-Loaded Mussel-Inspired Hydrogel with Wet Adhesion, Photothermal Antimicrobial, and In Situ Remineralization Capabilities for Caries Prevention, *Adv. Sci.*, 2024, **11**(45), e2409155.

14 Z. Mu, T. Jin, T. Chu, H. Lu, Y. Chen, S. Li, *et al.*, Functionalized MoS(2)-nanosheets with NIR-Triggered nitric oxide delivery and photothermal activities for synergistic antibacterial and regeneration-promoting therapy, *J. Nanobiotechnol.*, 2023, **21**(1), 463.

15 X. Cai, J. Tian, J. Zhu, J. Chen, L. Li, C. Yang, *et al.*, Photodynamic and photothermal co-driven CO-enhanced multi-mode synergistic antibacterial nanoplatform to effectively fight against biofilm infections, *Chem. Eng. J.*, 2021, 426.

16 Y. Zeng, X. Hu, Z. Cai, D. Qiu, Y. Ran, Y. Ding, *et al.*, Photodynamic and nitric oxide therapy-based synergistic

antimicrobial nanoplatform: an advanced root canal irrigation system for endodontic bacterial infections, *J. Nanobiotechnol.*, 2024, **22**(1), 213.

17 X. Hu, Y. Y. Huang, Y. Wang, X. Wang and M. R. Hamblin, Antimicrobial Photodynamic Therapy to Control Clinically Relevant Biofilm Infections, *Front. Microbiol.*, 2018, **9**, 1299.

18 J. Zhu, J. Tian, C. Yang, J. Chen, L. Wu, M. Fan and X. Cai, L-Arg-Rich Amphiphilic Dendritic Peptide as a Versatile NO Donor for NO/Photodynamic Synergistic Treatment of Bacterial Infections, Promoting Wound Healing, *Small*, 2021, **17**(32), e2101495.

19 J. C. Castillo-Martínez, G. A. Martínez-Castañón, F. Martínez-Gutierrez, N. V. Zavala-Alonso, N. Patiño-Marín, N. Niño-Martinez, *et al.*, Antibacterial and antibiofilm activities of the photothermal therapy using gold nanorods against seven different bacterial strains, *J. Nanomater.*, 2015, **16**(1), 177.

20 A. G. Al-Bakri and N. N. Mahmoud, Photothermal-Induced Antibacterial Activity of Gold Nanorods Loaded into Polymeric Hydrogel against *Pseudomonas aeruginosa* Biofilm, *Molecules*, 2019, **24**, 2661.

21 K. Bilici, A. Muti, F. Demir Duman, A. Sennaroglu and H. Yagci Acar, Investigation of the factors affecting the photothermal therapy potential of small iron oxide nanoparticles over the 730–840 nm spectral region, *Photochem. Photobiol. Sci.*, 2018, **17**(11), 1787–1793.

22 K. Bilici, N. Atac, A. Muti, I. Baylam, O. Dogan, A. Sennaroglu, *et al.*, Broad spectrum antibacterial photodynamic and photothermal therapy achieved with indocyanine green loaded SPIONs under near infrared irradiation, *Biomater. Sci.*, 2020, **8**(16), 4616–4625.

23 Q. Fang, K. Xu, Q. Xiong, Y. Xu, A. Hui and S. Xuan, Fe 3 O 4–Au–polydopamine hybrid microcapsules with photothermal–photodynamic synergistic anti-bacterial performance, *CrystEngComm*, 2021, **23**(37), 6610–6619.

24 X. Dai, Y. Zhao, Y. Yu, X. Chen, X. Wei, X. Zhang and C. Li, All-in-one NIR-activated nanoplatforms for enhanced bacterial biofilm eradication, *Nanoscale*, 2018, **10**(39), 18520–18530.

25 J. Wu, H. Han, Q. Jin, Z. Li, H. Li and J. Ji, Design and Proof of Programmed 5-Aminolevulinic Acid Prodrug Nanocarriers for Targeted Photodynamic Cancer Therapy, *ACS Appl. Mater. Interfaces*, 2017, **9**(17), 14596–14605.

26 A. Casas, Clinical uses of 5-aminolaevulinic acid in photodynamic treatment and photodetection of cancer: A review, *Cancer Lett.*, 2020, **490**, 165–173.

27 R. F. Donnelly, P. A. McCarron and A. D. Woolfson, Derivatives of 5-aminolevulinic Acid for photodynamic therapy, *Perspect. Med. Chem.*, 2007, **1**, 49–63.

28 K. Onbasli, G. Demirci, F. Isik, E. G. Durmusoglu, H. V. Demir and H. Y. Acar, Aqueous colloidal nanoplatelets for imaging and improved ALA-based photodynamic therapy of prostate cancer cells, *Chem. Commun.*, 2023, **59**(70), 10512–10515.

29 M. Hashemkhani, M. Loizidou, A. J. MacRobert and H. Yagci Acar, One-Step Aqueous Synthesis of Anionic and Cationic AgInS(2) Quantum Dots and Their Utility in Improving the Efficacy of ALA-Based Photodynamic Therapy, *Inorg. Chem.*, 2022, **61**(6), 2846–2863.

30 K. Onbasli, M. Erkisa, G. Demirci, A. Muti, E. Ulukaya, A. Sennaroglu and H. Yagci Acar, The improved killing of both androgen-dependent and independent prostate cancer cells by etoposide loaded SPIONs coupled with NIR irradiation, *Biomater. Sci.*, 2022, **10**(14), 3951–3962.

31 A. Sennaroglu, M. Khan, M. Hashemkhani and H. Yagci Acar, Determination of the Wavelength-Dependent Photothermal Conversion Efficiency of Photosensitizers for Photothermal Therapy: Application to Ag(2)S-Glutathione Quantum Dots, *J. Phys. Chem. B*, 2021, **125**(42), 11650–11659.

32 J. H. Merritt, D. E. Kadouri and G. A. O'Toole, Growing and analyzing static biofilms, *Curr. Protoc. Microbiol.*, 2006, DOI: **10.1002/9780471729259.mc01b01s00**.

33 P. S. Stewart and J. W. Costerton, Antibiotic resistance of bacteria in biofilms, *Lancet*, 2001, **358**(9276), 135–138.

34 Y. Wang, Y. Wang, Y. Wang, C. K. Murray, M. R. Hamblin, D. C. Hooper and T. Dai, Antimicrobial blue light inactivation of pathogenic microbes: State of the art, *Drug Resistance Updates*, 2017, **33–35**, 1–22.

35 S. U. Khan, G. O. Eren, N. Atac, A. Onal, M. H. Qureshi, F. K. Cooper, T. Almammadov, S. Kolemen, M. Sahin, F. Can and S. Nizamoglu, Antibacterial type-II InP/ZnO quantum dots via multimodal reactive oxygen species, *Chem. Eng. J.*, 2023, **480**, 148140.

36 Y. H. Lu, H. Wu, H. H. Zhang, W. S. Li and A. C. K. Lai, Synergistic disinfection of aerosolized bacteria and bacteriophage by far-UVC (222 nm) and negative air ions, *J. Hazard. Mater.*, 2023, **441**, 129876.

37 C. Montanari, D. I. Serrazanetti, G. Felis, S. Torriani, G. Tabanelli, R. Lanciotti and F. Gardini, New insights in thermal resistance of staphylococcal strains belonging to the species Staphylococcus epidermidis, Staphylococcus lugdunensis and Staphylococcus aureus, *Food Control*, 2015, **50**, 605–612.